AIAA 80-0389R

A New Approach in Cascade Flow Analysis Using the Finite Element Method

E. Baskharone* and A. Hamed†
University of Cincinnati, Cincinnati, Ohio

A new approach in analyzing the potential flow past cascades and single airfoils using the finite-element method is developed. In this analysis, the circulation around the airfoil is not externally imposed but is directly computed in the numerical solution. Different finite-element discretization patterns, orders of piecewise approximation, and grid sizes are used in the solution. The results obtained are compared with existing experimental measurements and exact solutions in cascades and single airfoils.

Nomenclature

A = area of a finite element
ℓ = contour length of a finite element
$\bar{n}$ = normal unit vector
N = shape functions defined over a finite element
p = number of nodes associated with a finite element
S = total number of finite elements having one or more nodes on one branch of the splitting boundary
$\bar{V}$ = velocity vector
V_{n_0} = velocity component normal to the exit station
x,y = spatial coordinates
Γ = circulation around a lifting body
ρ = flow density
ϕ = velocity potential

Subscripts & Superscripts

i = value of a variable at the ith node
e = finite element

I. Introduction

SEVERAL methods are available for the analytical solution of the potential flow through cascades of blades and around single airfoils. Some analytical methods are based on the use of conformal transformation.[1-5] These methods generally involve one transformation or a series of transformations to map the flow region into the exterior of a circle,[1-3] or a cascade of flat plates.[4,5] In the singularity methods, distributed sources, sinks and/or vortices[6] are placed on the airfoil surface and used to compute the blade flow velocity. Cascade flowfields have been successfully studied using the streamline curvature method,[7] the finite difference,[8] and the finite element methods.[9-12]

Regardless of the method of solution, the determination of circulation around the lifting body is basically a matter of primary concern for a unique potential field to exist. A unique value of the circulation can be determined for an airfoil with a sharp trailing edge through the application of the Kutta-Joukowski condition. This is not valid in most practical applications, in which case, other conditions representing a generalized form of this condition have been proposed as alternatives.[9,12,13] In the numerical solution of the flowfield, the trailing edge condition is usually satisfied iteratively leading to an approximate circulation value.[9,14]

The present analysis offers a new concept in handling potential flowfields with lifting airfoils. The problem is formulated in terms of the potential function, and the numerical solution is based on the use of the finite element method. This analysis deviates from previous ones in the inclusion of the circulation around lifting bodies as a nodeless degree of freedom to be evaluated in the finite element solution. This directly provides the unique solution without any externally imposed constraints.

II. Analysis

The problem is formulated in terms of the velocity potential ϕ as the primary variable. In this case, the velocity vector $\bar{V}$ is expressed in terms of ϕ as follows:

$$\bar{V} = \nabla\phi \tag{1}$$

The introduction of the above relation into the equation of conservation of mass, for steady flow, gives rise to the following equation:

$$\nabla \cdot (\rho \nabla \phi) = 0 \tag{2}$$

which, for an incompressible flow, assumes the Laplacian form:

$$\nabla^2 \phi = 0 \tag{3}$$

A. Solution Domain

Figure 1 shows the domain used in the numerical solution of the flowfield around a single airfoil. Two of the domain boundaries are oriented in the direction of the freestream and located far enough from the airfoil to justify the application of undisturbed flow conditions. The other two boundaries are placed far enough upstream and downstream of the airfoil for uniform inlet and exit flow conditions to exist. Generally, the velocity potential field is multivalued in this multiply connected domain due to the lift generated by the airfoil. The circulation around the airfoil represents the difference between the multivalues at any given point in the flowfield. However, a unique solution can be obtained by converting the flow region into a simply connected domain through the introduction of a splitting boundary which extends from the airfoil surface to one of the boundaries. This is represented in Fig. 1 by a pair of infinitesimally close lines extending from the airfoil trailing edge to the flow exit station. It should be noted that any other shape and position of this splitting boundary can serve the same purpose as long as it converts the

Presented as Paper 80-0389 at the AIAA 18th Aerospace Sciences Meeting, Pasadena, Calif., Jan. 14-16, 1980; submitted Jan. 21, 1980; revision received May 14, 1980.

*Graduate Research Assistant, Dept. of Aerospace Engineering and Applied Mechanics, presently with AiResearch Manufacturing Company of Arizona, Phoenix, Arizona. Student Member AIAA.

†Associate Professor, Dept. of Aerospace Engineering and Applied Mechanics. Member AIAA.

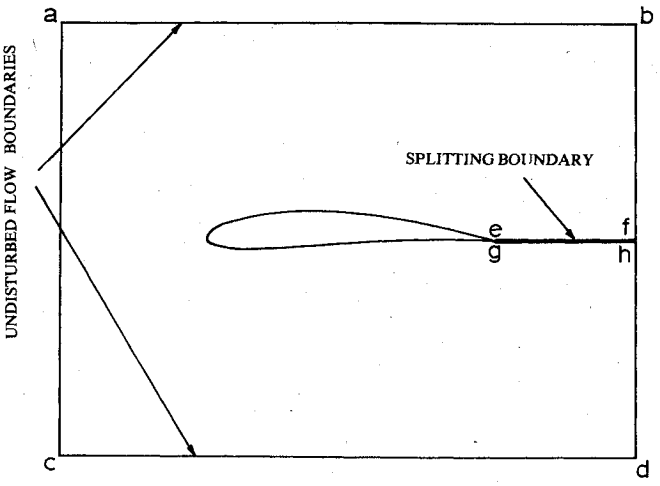

Fig. 1 Solution domain for a single airfoil.

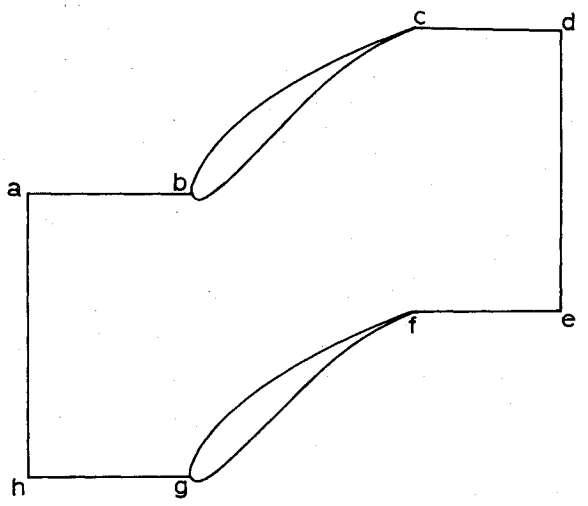

Fig. 2 Blade-to-blade cascade channel.

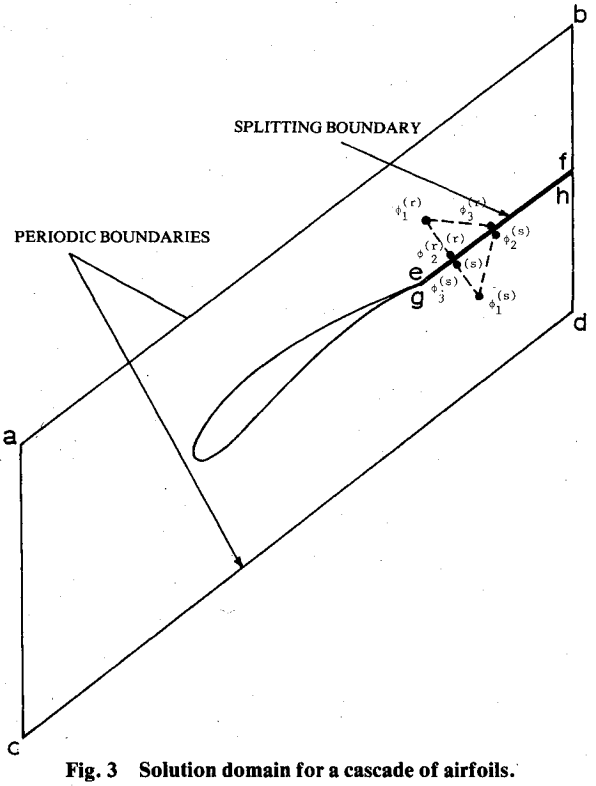

Fig. 3 Solution domain for a cascade of airfoils.

flow region into a simply connected domain. An abrupt change is allowed across this splitting boundary in the potential function, but not in the velocity field. The value of the potential jump across this boundary is introduced as an additional variable to be determined along with the discrete nodal values of the potential function in the finite-element solution.

The solution domain traditionally used in cascade flow numerical analyses is shown in Fig. 2. In addition to the blade-to-blade channel between two successive airfoils, the domain includes two other regions that extend upstream and downstream to the inlet and exit stations. The latter two are bounded by geometrically similar lines ba and gh from the airfoils leading edges and cd and fe from the airfoils trailing edges. In a stream function formulation, the value of the normalized stream function is usually taken zero over gf, the lower airfoil's upper surface, and one over bc, the upper airfoil's lower surface. The difference between the values of the normalized stream function at the corresponding points on the periodic boundaries ab and hg and also cd and fe is equal to one. If the same domain is used in the potential function formulation, the difference between the values of the potential function at the corresponding points on ab and hg, will not be the same as on cd and fe. This becomes clear when the flowfield is viewed instead in the domain shown in Fig. 3, in which the airfoil is located between the geometrically similar lines ab and cd which are separated by one pitch in the direction of the cascade front. This is the domain used in the cascade problem solution using the present potential function formulation.

B. Boundary Conditions

Referring to Figs. 1 and 3, four different types of boundary conditions are involved in the present problem. First, a linear velocity potential profile is specified at the inlet station in accordance with the uniform inlet conditions. When the flow is perpendicular to the inlet station, this Dirichlet-type boundary condition reduces to a uniform velocity potential along the inlet station.

The velocity component normal to the boundaries is known along the airfoil surface, where it is equal to zero when there is no flow injection. In addition, in the case of a single airfoil, the velocity normal to ab and cd is also equal to zero since these boundaries are parallel to the undisturbed flow direction,

$$\frac{\partial \phi}{\partial n} = 0 \tag{4}$$

over the airfoil surface and over ab and cd in the case of single airfoil. A uniform velocity V_{n_0} is specified at the exit station according to the principal of conservation of mass,

$$\frac{\partial \phi}{\partial n} = V_{n_0} \tag{5}$$

over bf and hd.

The third type of boundary conditions represents the solution periodicity over the boundaries ab and cd in Fig. 3. This boundary condition is handled in a manner similar to that of Ref. 10. Finally, the equality of the potential gradient on the opposite sides of the splitting boundary is discussed in Sec. II.D.

C. Galerkin's Finite-Element Formulation

The first step in a finite-element analysis is to discretize the solution domain into a number of finite elements. A potential-interpolating function is then assumed in each element as follows:

$$\phi^{(e)} = \sum_{i=1}^{p} N_i(x,y)\phi_i \tag{6}$$

where $[N_i,\ i=1,p]$ are known as the shape functions associated with the p nodes of the element e, and $[\phi_i,\ i=1,p]$ are the corresponding nodal values of ϕ. The substitution of this approximating function into the governing equation (3), results in a residual which, by Galerkin's method, is required to be orthogonal to the shape functions.[15] This leads to the following finite-element equation:

$$\int_{A^{(e)}} \left[\frac{\partial N_i}{\partial x}\frac{\partial N_j}{\partial x}+\frac{\partial N_i}{\partial y}\frac{\partial N_j}{\partial y}\right]^{(e)} \phi_j^{(e)}\,dA = \int_{\ell^{(e)}} N_i^{(e)}\frac{\partial \phi^{(e)}}{\partial n}\,d\ell \quad i=1,2,\ldots,p \tag{7}$$

where $A^{(e)}$ and $\ell^{(e)}$ refer to the area and contour of the element e.

D. The Circulation as a Nodeless Variable

The value of ϕ at any point on one branch of the splitting boundary differs from the value of ϕ at an infinitesimally close point on the other branch by a constant Γ. This constant is equal in magnitude to the circulation around the airfoil, and is introduced in the finite element algorithm as an additional variable. In contrast to the potential discrete values, this variable is not connected to any particular node but rather to the entire splitting boundary. The discrete potential values on one branch of this boundary can, therefore, be replaced in the global vector of unknowns by those values on the other branch plus the circulation Γ.

The introduction of circulation in the manner explained above serves two purposes. First, a unique solution is now possible upon the solution of the final set of equations which involves Γ as an unknown. Secondly, the requirement of a continuous velocity field across the splitting boundary is implicitly imposed as far as the velocity component along the boundary is concerned. This result is obvious since the potential jump across the splitting boundary is uniform. The continuity of the velocity vector is achieved through equating the normal velocity component on both sides of that boundary.

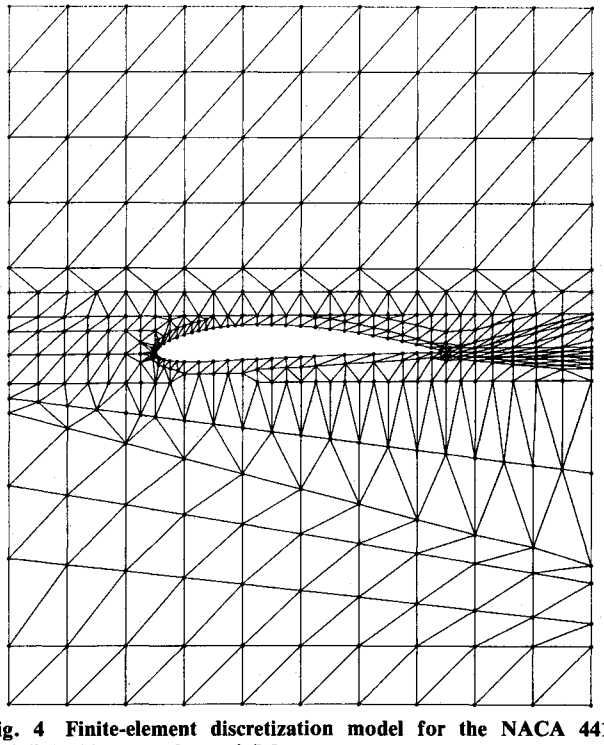

Fig. 4 Finite-element discretization model for the NACA 4412 airfoil, incidence angle = −0.5 deg.

The details of including Γ as a variable in the system of finite element equations is outlined below for the case of a simple triangular finite element. Referring to Fig. 3, the potential-interpolating function through the element s in the figure can be expressed as follows:

$$\phi^{(s)} = N_1^{(s)}\phi_1^{(s)} + N_2^{(s)}\phi_2^{(s)} + N_3^{(s)}\phi_3^{(s)}$$
$$= N_1^{(s)}\phi_1^{(s)} + N_2^{(s)}\phi_3^{(r)} + N_3^{(s)}\phi_2^{(r)} + N_4^{(s)}\Gamma \tag{8}$$

where

$$N_4^{(s)} = N_2^{(s)} + N_3^{(s)} \tag{9}$$

The coefficient of Γ in expression (8) has a nonzero value only for the subgroup of elements with one or two nodes on the branch gh in this case. In the general case where an element (s) with p nodes is used, the shape function associated with Γ is denoted $N_{p+1}^{(s)}$, where:

$$N_{p+1}^{(s)} = \sum_j N_j^{(s)} \tag{10}$$

and the summation extends over all the element nodes existing on this branch of the splitting boundary.

The residual in each of these elements is required by Galerkin's approach to be piecewise orthogonal to the shape function associated with Γ. In the global form, this condition can be expressed as follows:

$$\sum_{s=1}^{S}\int_{A^{(s)}}\left[\frac{\partial N_{p+1}^{(s)}}{\partial x}\frac{\partial N_k^{(s)}}{\partial x}+\frac{\partial N_{p+1}^{(s)}}{\partial y}\frac{\partial N_k^{(s)}}{\partial y}\right]\psi_k^{(s)}\,dA = \sum_{s=1}^{S}\int_{\ell^{(s)}} N_{p+1}^{(s)}\frac{\partial \phi^{(s)}}{\partial n}\,d\ell \quad k=1,2,\ldots,p+1 \tag{11}$$

where S represents the total number of elements with Γ as a nodeless degree of freedom. The array of unknowns $\psi_k^{(s)}$ in Eq. (11) includes the potential nodal values of element (s) excluding those on the branch gh. The array instead includes the corresponding ϕ values on the other branch as well as the circulation Γ. The local normal velocity $\partial\phi^{(s)}/\partial n$ along this branch is expressed in terms of the nodal values of the velocity potential on the opposite side of the splitting boundary. The derivatives of N_{p+1} can be evaluated from Eq. (10) as:

$$\frac{\partial N_{p+1}^{(s)}}{\partial x} = \sum_j \frac{\partial N_j^{(s)}}{\partial x} \tag{12a}$$

and

$$\frac{\partial N_{p+1}^{(s)}}{\partial y} = \sum_j \frac{\partial N_j^{(s)}}{\partial y} \tag{12b}$$

An alternative variational approach[15] can be followed to arrive at the same form of Eq. (11). In this case, the equation corresponds to making a functional $I(\phi_i,\Gamma,x,y)$ stationary with respect to the variable Γ, where:

$$I = \sum_{s=1}^{S}\int_{A^{(s)}}\left[\left(\frac{\partial\phi^{(s)}}{\partial x}\right)^2+\left(\frac{\partial\phi^{(s)}}{\partial y}\right)^2\right]dA - \sum_{s=1}^{S}\int_{\ell^{(s)}}\phi^{(s)}\frac{\partial\phi^{(s)}}{\partial n}\,d\ell \tag{13}$$

Only the elements having Γ as a degree of freedom will contribute to $\partial I/\partial\Gamma$.

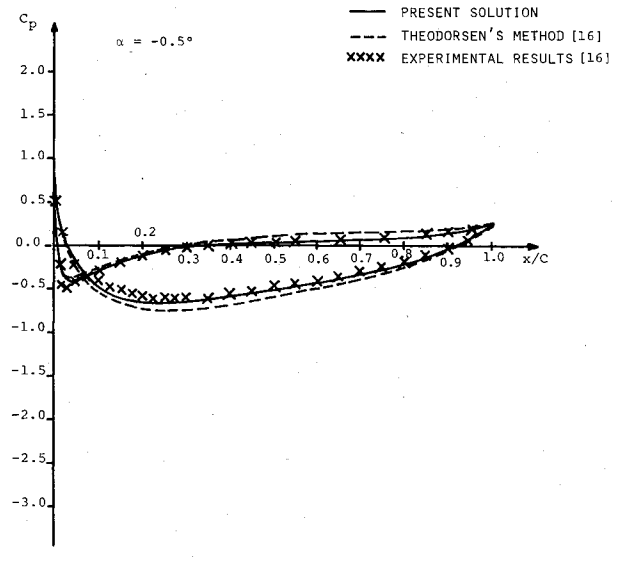

Fig. 5 Pressure coefficient for the NACA 4412 airfoil, incidence angle = −0.5 deg.

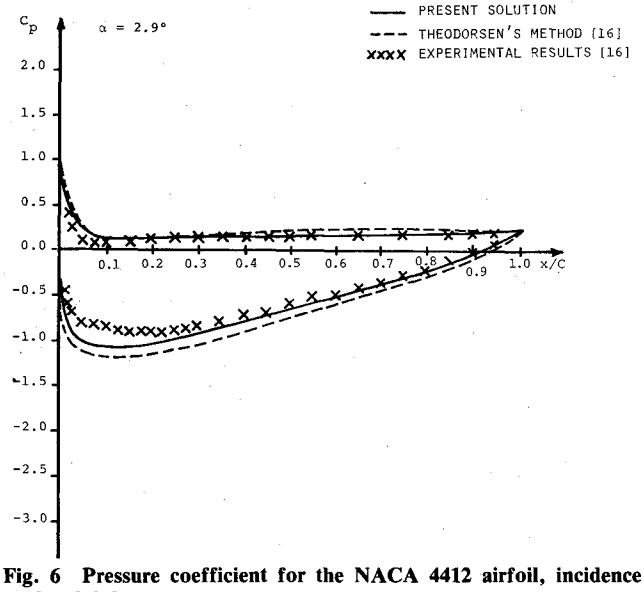

Fig. 6 Pressure coefficient for the NACA 4412 airfoil, incidence angle = 2.9 deg.

III. Results and Discussion

This section presents the results of applying the analysis to isolated airfoils and cascades for which analytical or experimental results exist. The first set of results corresponds to the flow around an isolated NACA 4412 airfoil. The data used in the comparison were reported in Ref. 16 for a range of incidence angles. The analytical results of this reference were obtained using Theodorsen's conformal transformation method.[2] The comparison of the results are presented at three different incidence angles of −0.5, 2.9, and 6.4 deg. In all three cases, the undisturbed flow conditions were applied in the numerical solution at the two horizontal lines which were placed 1.5 times the chord length, above and below the center of the leading edge. The finite-element discretization model is shown in Fig. 4. A total of 410 nodal points were located as shown in this figure and used to generate linear triangular elements. The desire to reduce the size of the element near the airfoil, coupled with the limited number of points defining the airfoil contour in Ref. 16, resulted in elements with a high aspect ratio in this region. Figures 5, 6, and 7 show the computed airfoil pressure distribution at −0.5, 2.9, and 6.4 deg incidence angles, respectively. The analytical results of

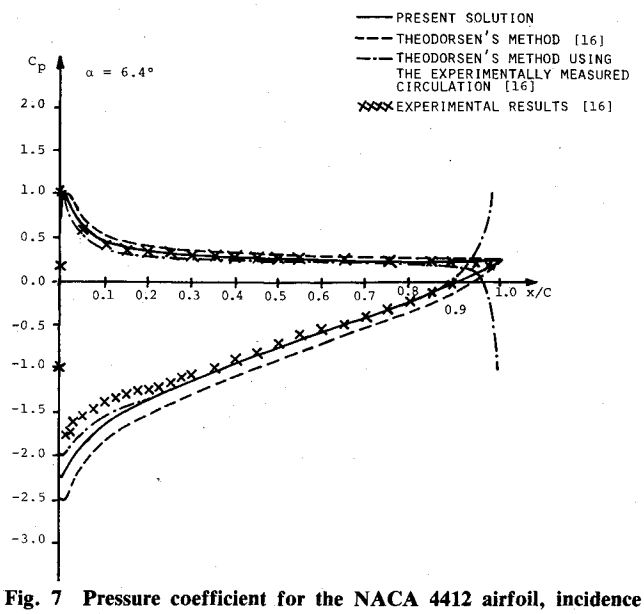

Fig. 7 Pressure coefficient for the NACA 4412 airfoil, incidence angle = 6.4 deg.

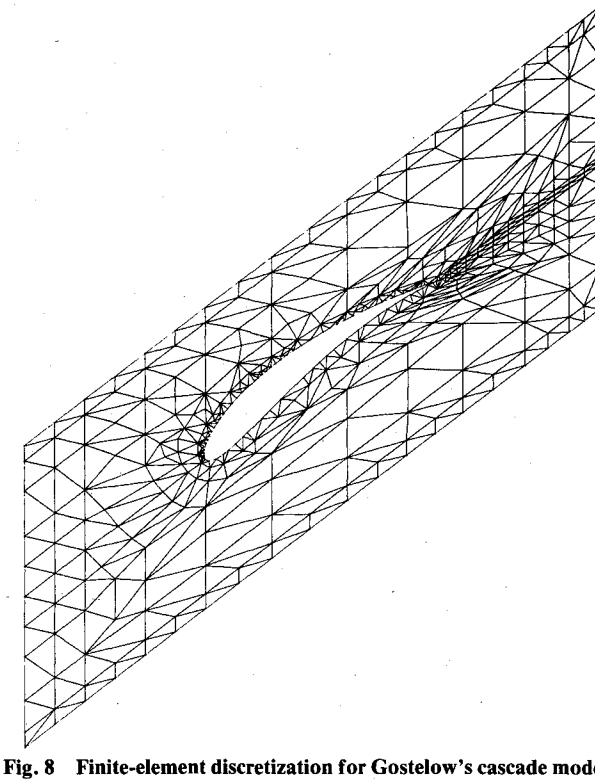

Fig. 8 Finite-element discretization for Gostelow's cascade model I.

Ref. 16 and experimental data reported in the same reference are also shown in these figures. The Kutta condition for a sharp trailing edge was used in Ref. 16 to obtain the results which are reproduced in Figs. 5-7. It can be seen from these figures that our results are in closer agreement with the experimental measurements than the results obtained using Theodorsen's method. Pinkerton[16] repeated the calculations at a 6.4 deg incidence angle using the experimentally measured lift to specify the circulation. The results of these computations are represented by the dash-dot curve in Fig. 7, in which the experimental data and the results of the present analysis are also shown for comparison. It can be seen from this figure that using the experimentally measured lift generally improves the agreement between the computed results using Theodorsen's method and the experimental measurements, except in the vicinity of the trailing edge. Our

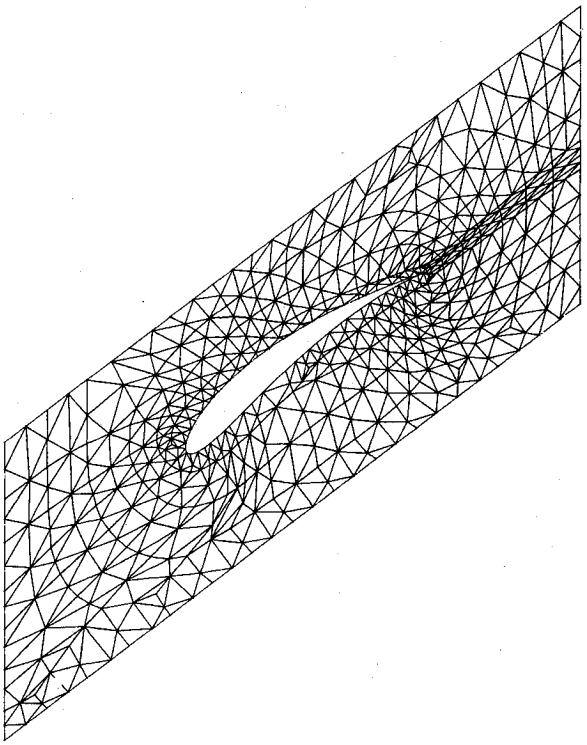

Fig. 9 Finite-element discretization for Gostelow's cascade model II.

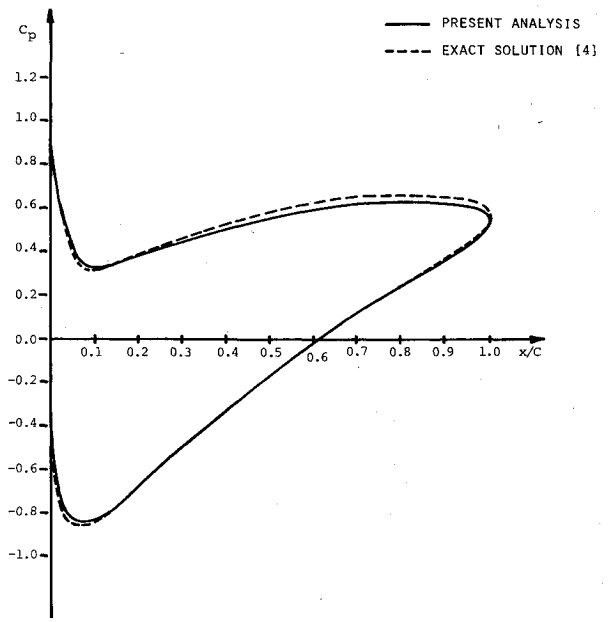

Fig. 11 Pressure coefficient for Gostelow's cascade using discretization model II.

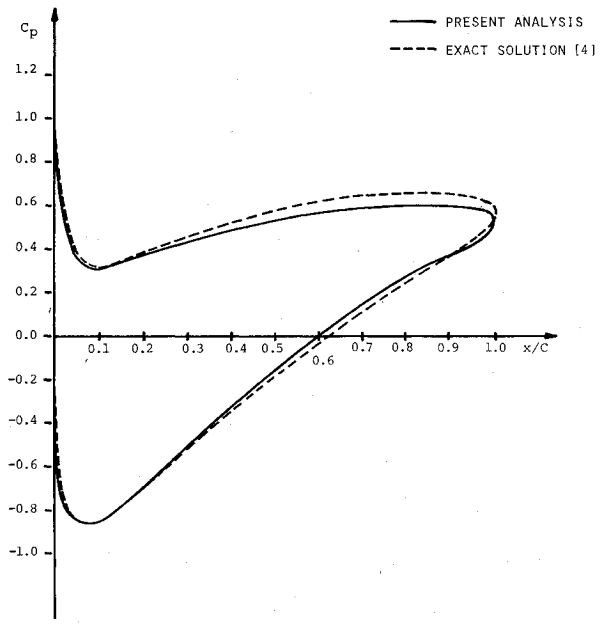

Fig. 10 Pressure coefficient for Gostelow's cascade using discretization model I.

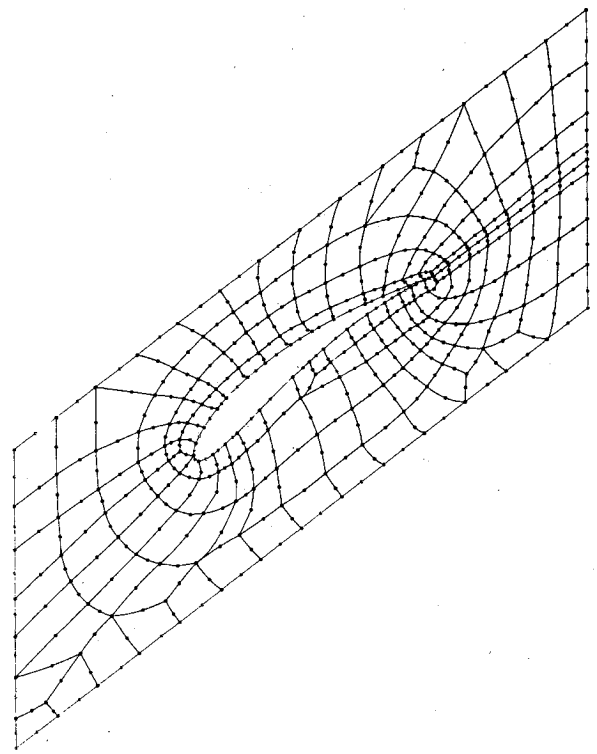

Fig. 12 Finite-element discretization model III for Gostelow's cascade.

results are still in closer agreement with the experimental measurements over all of the airfoil pressure surface and the airfoil trailing edge, but not near the leading edge on the suction side. An examination of Fig. 4 reveals that a coarser discretization pattern was generally used at the airfoil suction surface compared to the pressure side, particularly near the airfoil leading edge. We feel that a more refined mesh in this region would bring closer agreement between our computed results and the experimental data.

The second application of the present analysis was carried out in the cascade geometry of Ref. 4. This is a cascade for which the airfoil geometry and pressure distribution were obtained by Gostelow, through the application of Merchant and Collar transformation[5] to a set of ovals. The generated airfoil in this cascade has a pitch-chord ratio (s/c) of 0.9901573 and a stagger angle of 37.5 deg, and the flow inlet angle is 53.5 deg. Two different finite-element discretization models with the linear triangular elements were used in the solution. These models are shown in Figs. 8 and 9. In the first model, a total of 431 nodes were placed in the flow region, as shown in Fig. 8 with a total of 691 elements. The second model (Fig. 9) involved a larger number of nodes and elements (624 and 1074, respectively). The first discretization model of Fig. 8 includes elements with high aspect ratio near the boundaries. The results of these two discretization models will be compared to investigate this effect. The computed

Table 1 Comparison of the discretization models

Case	Element type	Precision of numerical computations	No. of nodes	No. of elements	Core size, kilobytes	CPU, s	ϵ, deg
1	Linear triangular element	Double precision	431	691	269	12	+2.078
2	Linear triangular element	Double precision	624	1074	457	16	+0.517
3	Parabolic quadrilateral isoparametric element	Single precision	624	179	779	628	−0.376

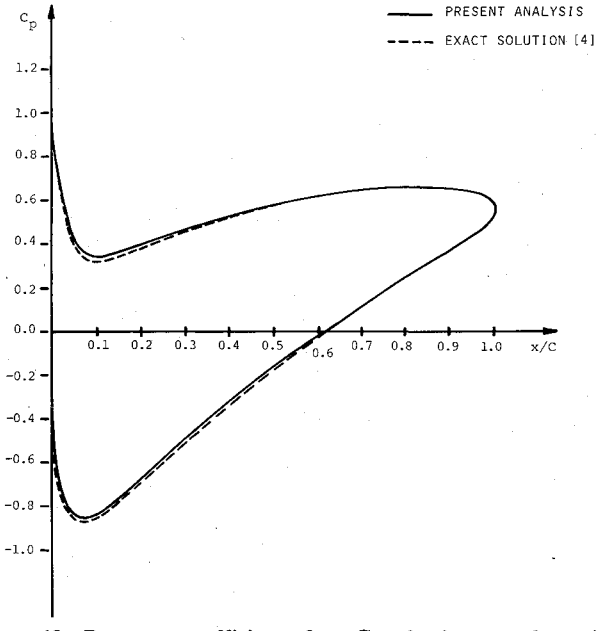

Fig. 13 Pressure coefficient for Gostelow's cascade using discretization model III.

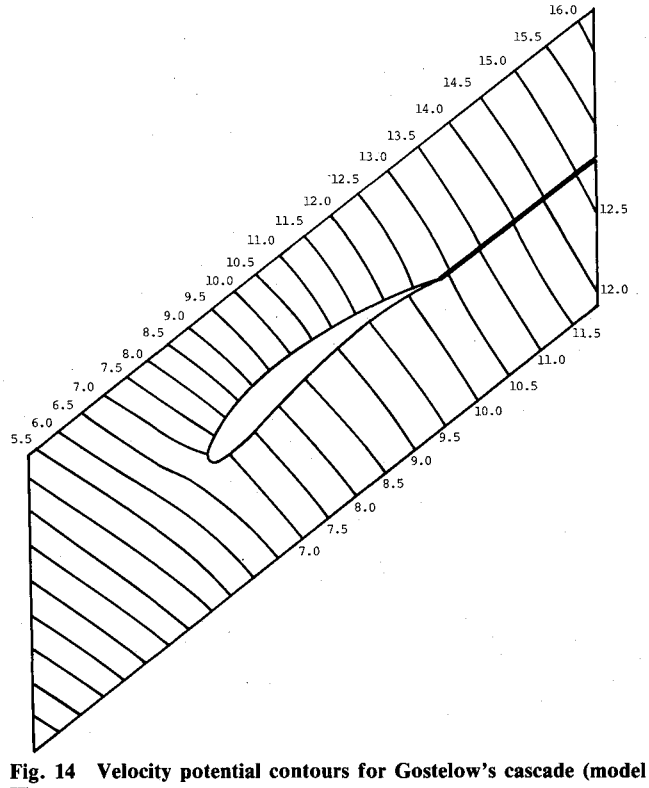

Fig. 14 Velocity potential contours for Gostelow's cascade (model II).

results corresponding to both cases are shown in Figs. 10 and 11. Gostelow's exact solution[4] is also reproduced on the same figures. It can be seen from these figures that the discretization pattern of Fig. 9 results in a noticeable improvement in the airfoil pressure distribution near the trailing edge and in particular over the pressure surface. The improvement is attributed to the more regular grid pattern in Fig. 9.

The flowfield in the same cascade was also computed using parabolic quadrilateral isoparametric elements[15] according to the discretization pattern shown in Fig. 12. The nodal numbers and locations used with the linear triangular discretization pattern of Fig. 9 were maintained with the isoparametric elements which resulted in a total of 179 elements. The computed pressure distribution along the blade is shown for this case in Fig. 13, and the corresponding velocity potential contours are shown in Fig. 14. Comparing Figs. 11 and 13, the airfoil pressure distribution obtained with the isoparametric element is seen to be in closer agreement with the exact solution. This is the result of the higher order of approximation provided by this element.The CPU time associated with this case is, however, much higher. The difference between the values of the velocity potential on the two branches of the splitting boundary can be seen clearly in Fig. 14.

The results of Figs. 10, 11, and 13 are of particular interest because of the existence of an exact solution for this cascade. The flow exit angle is chosen as a basis for comparison, since it is directly related to the circulation around the airfoil. The exit flow angle was equal to 30.013 deg in Gostelow's exact solution and is equal to 32.091, 30.530, and 29.637 for the discretization models of Figs. 8, 9, and 12, respectively. A comparison of these models in terms of CPU time and storage requirement using an AMDAHL 470 computer is given in Table 1. The isoparametric element computations were performed on a single precision basis because of core size considerations. The difference between the computed average flow angle at the exit section and the exact exit flow angle is given as ϵ in the last column of Table 1. The noticeable reduction of ϵ in case 2 compared to case 1 cannot be justified by the increased number of elements, but attributed mostly to the more regular grid pattern of Fig. 9. One can also infer the importance of the more regular grid in comparing Figs. 10 and 11.

Several conclusions can be drawn in light of the data in Table 1. The linear element is found to be highly efficient in terms of the computation time. This is due to the relative simplicity of evaluating this element stiffness matrix. In the case of the parabolic element, more time is consumed in performing the numerical integration in the stiffness matrix. This is due to the higher-order terms in the shape functions and the coordinate transformation involved.[15] In addition, the core size used in the parabolic element solution is much higher than that of the linear element, for the same reasons, and also due to the large number of nonzero entries in each row of the global stiffness matrix in this case.

IV. Conclusions

A new approach in the solution of potential flow around isolated airfoils and in cascades has been developed. It is based on the use of the finite element method with the velocity potential as a primary field variable. The present analysis differs from previous studies in the inclusion of the circulation around the airfoil as a nodeless degree of freedom to be determined in the numerical solution.

The results of the numerical solution are presented for two basic problems, namely, a single NACA airfoil and a cascade of airfoils generated by conformal transformation. The computed results are compared with the available analytical solutions and experimental data to verify the circulation innovation.

The approach presented here can be applied without modification to any multiply connected flow domain with lifting bodies. It has been employed by the authors in the complex two-dimensional flowfield of a scroll nozzle assembly,[17] and also in the three-dimensional flowfield of a radial inflow turbine scroll.[18] These two applications serve to demonstrate the versatility and applicability of this new approach to other more complex flowfields. This represents a great advantage over the numerical solutions satisfying a specified approximate trailing edge condition.

Acknowledgment

This research was sponsored by NASA Grant No. NSG 2066, Lewis Research Laboratory, Cleveland, Ohio.

References

[1] Carter, A.D.S. and Huges, H. P., "A Theoretical Investigation into the Effect of Profile Shape on the Performance of Aerofoils in Cascade," Aeronautical Research Council, R&W 2884, 1946.

[2] Theodorsen, T., "Theory of Wing Sections of Arbitrary Shape," NACA Rept. No. 411, 1932.

[3] Goldstein, S., "Low Drag and Suction Airfoils," *Journal of the Aeronautical Sciences*, Vol. 15, 1948, pp. 189-220.

[4] Gostelow, J. P., "Potential Flow Through Cascades—A Comparison Between Exact and Approximate Solutions," Aeronautical Research Council, CP No. 807, 1965.

[5] Merchant, W. and Collar, A. R., "Flow of an Ideal Fluid Past a Cascade of Blades, Part II," Aeronautical Research Council, R&M No. 1893, May 1941.

[6] Martensen, E., "The Calculation of Pressure Distribution on a Cascade of Thick Airfoils by Means of Fredholm Integral Equations of the Second Kind," NASA TT F-702, July 1971.

[7] Bindon, J. P. and Carmichael, A. D., "Streamline Curvature Analysis of Compressible and High Mach Number Cascade Flows," *Journal of Mechanical Engineering Science*, Vol. 13, No. 5, Oct. 1971, pp. 344-357.

[8] Katsanis, T., "Fortran Program for Calculating Transonic Velocities on a Blade-to-Blade Stream Surface of a Turbomachine," NASA TN D-5427, Sept. 1969.

[9] Prince, T. C., "Prediction of Transonic Inviscid Steady Flow in Cascades by Finite Element Methods," Ph.D. Dissertation, Univ. of Cincinnati, 1976.

[10] Laskaris, T. E., "Finite Element Analysis of Three-Dimensional Potential Flow in Turbomachines," *AIAA Journal*, Vol. 16, July 1978, pp. 717-722.

[11] Thompson, D. S., "Finite Element Analysis of the Flow Through a Cascade of Aerofoils," Turbo/TR 45, Engineering Dept., Cambridge Univ., 1973.

[12] Schmid, G., "Incompressible Flow in Multiply Connected Regions," *Numerical Methods in Fluid Dynamics,* Proceedings of the International Conference held at the University of Southampton, England, Sept. 1973, pp. 153-171.

[13] Gostelow, J. P., "Trailing Edge Flows Over Turbomachine Blades and the Kutta Joukowski Condition," ASME Paper 75-GT-94, March 1975.

[14] De Vries, G. and Norrie, D. H., "The Application of the Finite Element Technique to Potential Flow Problems," *Journal of Applied Mechanics, ASME Transactions*, Dec. 1971, pp. 798-802.

[15] Zienkiewicz, O. C., *The Finite Element Method in Engineering Science*, McGraw Hill, London, 1971.

[16] Pinkerton, R. M., "Calculated and Measured Pressure Distributions Over the Midspan Sections of the NACA 4412 Airfoil," NACA Rept. No. 563, 1936.

[17] Hamed, A., Baskharone, E., and Tabakoff, W., "A Flow Study in Radial Inflow Turbine Scroll-Nozzle Assembly," *Journal of Fluids Engineering, ASME Transactions*, Vol. 100, March 1978, pp. 31-36.

[18] Hamed, A. and Baskharone, E., "Analysis of the Three-Dimensional Flow in a Turbine Scroll," *Journal of Fluids Engineering*, Vol. 102, Sept. 1980, pp. 297-301.